

Curvature and Torsion estimation of 3D functional data: A geometric approach to build the mean shape under the Frenet Serret framework

Juhyun Park^{1,2}, Nicolas Brunel^{1,2,3}, and Perrine Chassat¹

¹LaMME, Université Paris-Saclay, CNRS, France

²ENSIIE, Évry, France

³Quantmetry, Paris, France

March 7, 2022

Abstract

The analysis of curves has been routinely dealt with using tools from functional data analysis. However its extension to multi-dimensional curves poses a new challenge due to its inherent geometric features that are difficult to capture with the classical approaches that rely on linear approximations. We develop an alternative characterization of a mean that reflects shape variation of the curves. Based on a geometric representation of the curves through the Frenet-Serret ordinary differential equations, we introduce a new definition of mean curvature and mean torsion, as well as mean shape through the notion of mean vector field. This new formulation of the mean for multi-dimensional curves allows us to integrate the parameters for the shape features into the unified functional data modelling framework. We formulate the estimation problem of the functional parameters in a penalized regression and develop an efficient algorithm. We demonstrate our approach with both simulated data and real data examples.

Keywords: functional data analysis, curvature, torsion, shape analysis, ordinary differential equations, movement data.

1 Introduction

We consider the problem of analyzing a set of three-dimensional curves in \mathbb{R}^3 in the spirit of functional data analysis. A typical example would be the recordings of spatial coordinates for tracking movements of body parts or objects (e.g., [Flash and Hogan \(1985\)](#)). Our motivating example deals with the movements signals automatically captured by a motion capture system by the company MOCAPLAB¹. Among the many fields of exploration of motion capture is the very specific field of sign language involving movements of the body, hands, fingers, face and eyes and achieve a capacity for expression as rich and structured as that offered by speech ([Gibet et al., 2016](#)). An example of the sign signals as well as biomechanical experimental data ([Raket et al., 2016](#)) is depicted in Figure 1. These types of movement are challenging to study as they are meaningful but are difficult to characterize without specific knowledge in the field. Our aim

¹<https://www.mocaplab.com/fr/>

is to develop statistical tools to extract “primitives” or a template specific to the nature of the signals studied.

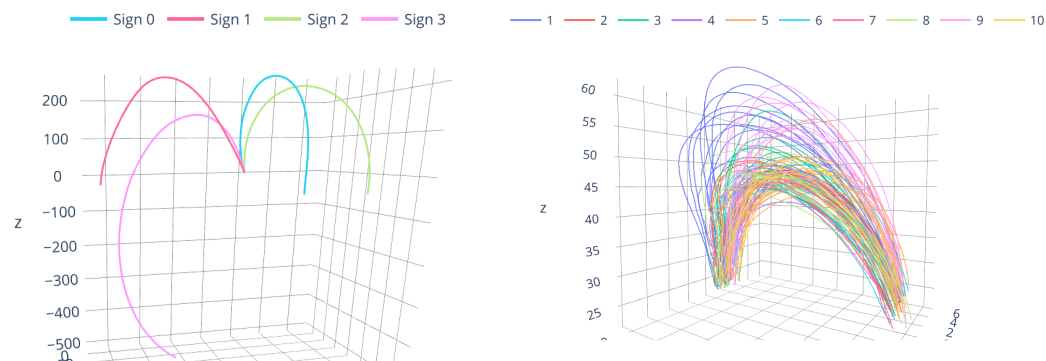


Figure 1: Motion signals: sign "FLY" (left) and hand movements from biomechanical experiments in [Raket et al. \(2016\)](#). (right). On the right, different colours represent different subjects.

It is of scientific interest to analyze three-dimensional curves in terms of curvature and torsion ([Lewiner et al., 2005](#); [Sangalli et al., 2009](#); [Kim et al., 2013](#)). Indeed, the geometry of the trajectories of movement have physical significance: curvature and torsion characterize this geometry and can provide insightful summaries of kinetic curves to scientists. This is a challenging task as curvature and torsion depend on higher order derivatives and their estimation from real data (even with a low noise) can be very unstable. Hence, the focus has been more on estimating derivatives in nonparametric regression and the link to functional data is somewhat lost.

On the other hand, certain geometric variation of curves, often in two or three-dimensions, is studied under shape analysis. A notion of shape is understood as what is left invariant under the actions of the rigid transformations of the Euclidean space, i.e., rescaling, translating and rotating. Viewing shapes as points on a manifold, shapes are formally defined as equivalence classes under some appropriate group actions. Several ways of constructing shape spaces (or feature spaces) have been proposed: discretization with landmarks based after discretization ([Dryden and Mardia, 1998](#)), or infinite dimensional shape spaces ([Younes, 2010](#); [Srivastava et al., 2011](#)). The classical statistical methodologies need to be adapted in order to deal with the non-Euclidean properties of shape spaces. Such shape analysis requires a definition of distance (inducing a Riemannian structure for instance) between points on a manifold and the natural extension of the usual mean is defined as a Fréchet mean. Some of these ideas, such as the elastic shape analysis has been suggested for analyzing the variations of functional data, typically for the registration problem in one-dimensional curves ([Kurtek et al., 2012](#)). Its extension to multi-dimensional curves is found in [Srivastava and Klassen \(2016\)](#). Under this framework, the main task is to estimate a geodesic on the manifold to quantify similarity of shapes. Hence, the variation of shapes tends to be limited to deformations on a geodesic and a statistical problem is somewhat hidden in the optimization problems. Also, the link to physical parameters is lost.

Our aim is to integrate both types of analysis in a unified framework to characterize a mean that respects the geometry of the curves and, at the same time, maintain the link to the physical parameters. We begin by treating multidimensional curves as a special instance of multivariate functional data. A standard assumption with functional data analysis (FDA) ([Ramsay and Silverman, 2005](#); [Ferraty and Vieu, 2006](#); [Wang et al., 2016](#)) is that there exists a common structure, often through a common mean and variance function, which then allows for a parsimonious decomposition of variability through functional principal component analysis. This type of linear

approximations is powerful as it allows us to naturally extend tools for univariate methods to multivariate ones (Chiou et al., 2014; Happ and Greven, 2018). These ideas were successfully applied to movements data (Goldsmith and Kitago, 2016; Backenroth et al., 2018). Nevertheless, such analytic extension can also hide some important features in these types of multivariate functional data (Dai and Genton, 2018). By borrowing ideas from statistical shape analysis (Dryden and Mardia, 1998; Kim et al., 2021), we develop an alternative characterization of the common structure that is linked to the common geometry of the curves, which can be viewed as a geometric mean. The notion of a geometric mean has been used in functional data analysis somewhat intuitively in defining *structural mean* in the presence of phase variation (Kneip and Gasser, 1992), more generally with manifold structure (Chen and Müller, 2012), and in detecting shape outliers in multivariate functional data (Dai and Genton, 2018). Recent developments in functional data analysis focus on generalizations beyond the Euclidean data by allowing for non-standard features such as data on a manifold or in a general metric space (Lin and Yao, 2019; Dubey and Müller, 2019; Petersen and Müller, 2019). Our approach is complimentary, as our generalization is to facilitate the Euclidean data analysis by incorporating non-Euclidean features, towards enhancing its interpretability.

We consider a new distance between curves that does not depend on the usual Cartesian coordinate system but uses a parameterization of the space of smooth curves based on a geometric curve representation. This representation provides a local orthonormal basis system and is shown to be related to the Frenet Ordinary Differential Equation (ODE). We treat this representation as a prototype of our statistical model and explicitly define shape variation and phase variation models under our new framework. We show that the solution of the ODE, the Frenet paths, can be interpreted as a representative of the equivalence class or *shape*. Within this framework, we introduce a new definition of mean shape through the mean ODE (or flow). In particular, we introduce the notion of mean curvature and mean torsion within this framework and show that the estimation of parameters can be cast into the problem of an ODE estimation in a Lie group (Hairer et al., 2006). To accompany the new definition of the mean, we propose a statistical framework for inference and develop an efficient algorithm. In general, the ODE estimation is a difficult problem (e.g., Ramsay et al. (2007)), especially when involving nonparametric estimation of time-varying parameters (e.g. Müller and Yao (2010); Ding and Wu (2014)), even without the orthogonality constraint required in our formulation. As a by-product, our formulation offers a new solution to a non-trivial ODE inference problem. We refer readers to Ramsay and Hooker (2017) for recent development on data analysis with ODE models.

The paper is organized as follows. Section 2 introduces fundamentals of the curve representation and reviews related concepts from elastic shape analysis. Section 3 develops new characterizations of a mean shape under our statistical framework. Section 4 presents our estimation algorithms, followed by numerical studies in Section 5. Main proofs, additional derivations and background materials are given in the supplementary. Our code is made available in the Python package `FrenetSerretMeanShape` (<https://github.com/perrinechassat/FrenetSerretMeanShape>).

2 A geometric representation of curves

We are interested in analysing a set of curves in \mathbb{R}^3 defined as functions $\{x : [0, T] \rightarrow \mathbb{R}^3\}$. In order to simplify the exposition, we assume that the curves are *regular*, *i.e.*, of class C^r , $r \geq 3$ (w.r.t time t) and the time derivative $\dot{x}(t)$ never vanishes on $[0, T]$. For notation, we write $\|\cdot\|$ for Euclidean norm in \mathbb{R}^p and $\|\cdot\|_2$ for L_2 functional norm.

2.1 Shape of the curve

For a curve x , the arclength is defined as $s(t) = \int_0^t \|\dot{x}(u)\|_2 du, t \in [0, T]$ and $s(T) = L$ is the total length of the curve $X = \{x(t), t \in [0, T]\}$. The *shape* of the curve $X : [0, L] \rightarrow \mathbb{R}^3$ is the image of the function x , which satisfies $x(t) = X(s(t))$. The derivation with respect to arclength s is denoted with prime i.e $Y'(s) = \frac{d}{ds}Y(s)$, whereas time differentiation is always denoted by a dot. For convenience, we use the arclength parametrization but the shape function is preserved under different parametrization of the curve, as demonstrated in Section 3.1. Our interest is in characterizing the variation of the shape function X in the population of curves x .

2.2 Curvature and Torsion

The curvature and torsion are geometric invariants of the curve, independent of the parametrization of a curve X . Moreover, they completely describe the local behaviour of the curve, in the sense that two curves with the same curvature and torsion are identical up to translation and rotation. That is, they are invariant under the action of rigid (Euclidean) motions. These functional parameters can be directly defined with extrinsic formulas as

$$\kappa(s(t)) = \frac{\|\dot{x}(t) \times \ddot{x}(t)\|}{\|\dot{x}(t)\|^3}, \quad \tau(s(t)) = \frac{\langle \dot{x}(t) \times \ddot{x}(t), \ddot{\ddot{x}}(t) \rangle}{\|\dot{x}(t) \times \ddot{x}(t)\|^2}. \quad (1)$$

Although the formulas are useful for computing curvature and torsion in practice, the geometrical interpretation of these parameters is somewhat hidden in these expressions.

2.3 Local representation of the curves and Frenet frames

As the point in the curve lies in \mathbb{R}^3 , we can define a three-dimensional basis for each point. The arclength parametrization of the curve $x(t) = X(s(t))$ implies that $\dot{x}(t) = \dot{s}(t)X'(s(t))$, meaning that the tangent vector $T(s) \triangleq X'(s)$ is unit length for all s in $[0, L]$. At points where $\|T(s)\| \neq 0$, since $\|T(s)\|^2 = 1$, the derivative $T'(s)$ is orthogonal to $T(s)$ and thus there exists a unit vector $N(s) \propto T'(s)$. The curvature can be defined as $s \mapsto \kappa(s) = \|T'(s)\|$, which measures how rapidly the curve pulls away from the tangent line. Adding this Normal vector $N(s) = \frac{1}{\kappa(s)}T'(s)$ together with the bi-normal vector $B(s) = T(s) \times N(s)$ to the tangent vector $T(s)$ defines a local orthonormal basis system in \mathbb{R}^3 . Viewing the local basis system as a function of s defines a moving frame, known as Frenet frames. The torsion $s \mapsto \tau(s)$ is the function that satisfies $B'(s) = -\tau(s)N(s)$ for all s in $[0, L]$, which measures how rapidly the curve pulls away from the osculating plane determined by the tangent vector and the normal vector. Physically, one can view that a curve can be obtained from a straight line by bending (curvature) and twisting (torsion) (Carmo, 1976).

2.4 Geometry of the curve and elastic shape analysis

Instead of treating the shape function X directly, elastic shape analysis (Srivastava et al., 2011; Srivastava and Klassen, 2016) treats curves x as a shape object, which are then compared with a geodesic distance between them defined through optimal deformations. A popular transformation is based on the square root velocity function (SRVF), defined for each curve $x(t) = X(s(t))$ as

$$q_x(t) = \frac{\dot{x}(t)}{\sqrt{\|\dot{x}(t)\|}}.$$

This can be viewed as a representation of the shape of the curve on a manifold. The distance between two curves is then defined as the L_2 distance between q_x and is parametrisation-independent.

The SRVF transformation $F : x \mapsto \dot{x}(t)/\sqrt{\|\dot{x}(t)\|}$ helps defining a pre-shape space that is used for characterizing the underlying shape of a given function. The pre-shape space for unit length open curves is $\mathcal{C}^O = \{q \in L^2([0, T], \mathbb{R}^p)\}$ and is simply the hypersphere of $L^2([0, 1], \mathbb{R}^p)$. The framework is better suited to explain the variation of curves in the presence of warping. Assume that two curves x_0, x_1 are similar in the sense that $x_1 \approx x_0 \circ h$ for a time warping function $h : [0, T] \rightarrow [0, T]$. In order to align the curves x_0, x_1 with SRVF, we solve the following minimisation problem that defines at the same time a geodesic distance:

$$d_{srvf}(x_0, x_1) = \inf_{O \in SO(3), h \in H_T} \int_0^T \left\| q_0(t) - O\sqrt{\dot{h}(t)}q_1(h(t)) \right\|^2 dt. \quad (2)$$

The distance d_{srvf} between two curves x_0 and x_1 is invariant to translation, rotation and reparametrisation. In the case of multiple curves, the SRVF mean $\tilde{\mu}_{srvf}$ is defined as a Fréchet mean that minimizes the average geodesic distance:

$$\tilde{\mu}_{srvf} = \arg \min_{\mu} \sum_{i=1}^n d_{srvf}(x_i, \mu). \quad (3)$$

An iterative algorithm is used to solve the optimization problem.

As the SRVF representation depends on the first derivative, it reflects some geometry of the curve. In fact, we can express $q_x(t) = \sqrt{\dot{s}(t)}T(s(t))$. The relation between T and κ as explained in section 2.3 implies that this representation implicitly depends on the curvature and, to less extent, on torsion. Brunel and Park (2019) extend this approach by incorporating the Frenet frames directly in the representation. Nevertheless, the dependence on the parameters is still implicit in this framework.

2.5 Illustration of interplay between curves and geometry

To appreciate the significance of curvature and torsion in the representation of curves, we illustrate the interaction between curves and geometry by a simplified example. We consider two set of 25 Euclidean curves, the first one with some variability only in the torsion and the second one only in the curvature, as shown in Figure 2. These curves satisfy the geometric curve representation with, for the first case, a constant curvature equal to 5 for all curves and a torsion $\tau_i(s) = -a_i 3 \sin(2\pi s), i = 1, \dots, 25$ with a_i equally spaced from -1 to 1 , for the second one, a constant torsion equal to 0 for all curves and a curvature $\kappa_i(s) = -a_i |3 \sin(\pi s)|, i = 1, \dots, 25$ with a_i equally spaced from -1 to 1 .

We compute the mean Euclidean curve by three different methods: the elastic mean by SRVF method (using the implementation in the package `fdasrsf` Tucker (2021), the arithmetic mean, and the proposed mean by "Frenet-Serret method", introduced in section 3. The results are shown in the first column of Figure 2. For two standard methods, there is no connection between the mean and the parameters so we compute the curvature and torsion of each of the means by extrinsic formulas (1) with estimated derivatives by local polynomial regression. The estimates are shown in the two last columns of Figure 2. It can be seen in the first case that the curvatures of the elastic and arithmetic means are no longer constant, but have a spike between 3 and 5 times larger. These two means do not respect the curvature and torsion of the different curves from which they are calculated. The idea of our method is to define a mean that respects the geometry of the curves in all cases. Indeed, the mean calculated by our "Frenet-Serret" method

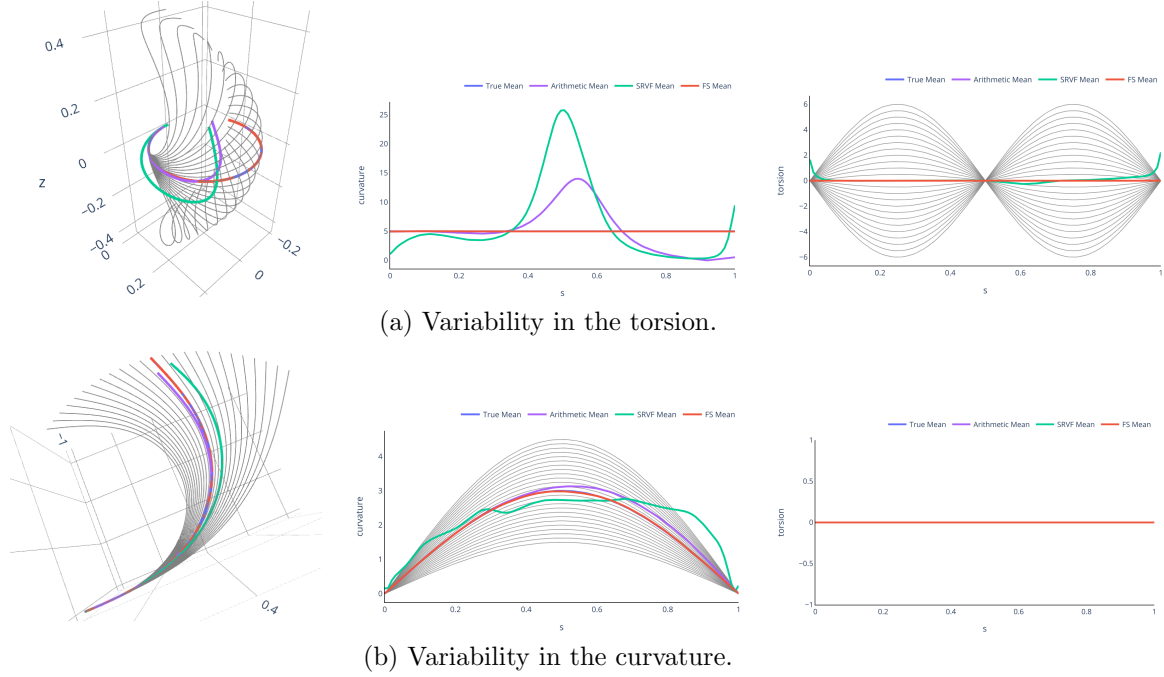


Figure 2: Set of Euclidean curves (first column), curvatures (second column), torsions (third column) overlaid with means: true mean in blue, elastic mean by SRVF in green, arithmetic mean in purple and the proposed mean by Frenet-Serret method in red.

has a constant curvature equals to 5 and a zero torsion. Although this example is contrived to demonstrate our motivation, this type of variability between curves can also be found in real data examples, presented in section 5.3.1.

3 Characterization of a Frenet-Serret mean shape

We develop a new framework to characterize a mean shape with an explicit parametrization of the curves linked to the geometry of the curves. Let us consider N curves in \mathbb{R}^3 defined as functions $\mathcal{S} = \{x_1, \dots, x_N\}$ from $[0, T]$ to \mathbb{R}^3 . For regular curves x_i , the shape function X_i is identified with the arclength parameterized curves as $x_i(t) = X_i(s_i(t))$, $i = 1, \dots, N$.

3.1 Sources of variation of the curves

The arclength parametrization should not be confused with the standard representation of time warping or phase variation in the functional data. Suppose that x_i is given as $x_i(t) = x(h_i(t))$, where $h_i \in H_T = \{h : [0, T] \rightarrow [0, T] | h(0) = 0, h(T) = T, h' \geq 0\}$ are warping functions. As $\dot{x}_i(t) = \dot{x}(h_i(t))\dot{h}_i(t)$, by change of variables, the corresponding arclength can be expressed as

$$s_i(t) = \int_0^t \|\dot{x}(h_i(t))\dot{h}_i(t)\| dt = \int_0^{h_i(t)} \|\dot{x}(u)\| du = s(h_i(t)).$$

It follows that $x_i(t) = x(h_i(t)) = X(s(h_i(t))) = X(s_i(t))$, that is, the *shape* of the curve is preserved under time warping. For univariate functional data, phase variation expressed as time

warping functions is often confounded with shape variation.

In this work, we distinguish between phase (h_i) and shape variation (X_i). As seen earlier, elastic shape analysis is adapted to phase variation. We explicitly model both types of variations in the spirit of functional data analysis and treat two cases separately

$$M_1 : x_i(t) = X_i(s_i(t)), \quad M_2 : x_i(t) = X_i(s_i(h_i(t))). \quad (4)$$

As the latter can be viewed as an extension of the former, we first develop our characterization of mean shape for M_1 . An extension to M_2 is presented in section 3.7.

3.2 Shape function and its equivalent class

We have seen in section 2.3 that associated with the shape X is the Frenet frames T, N, B , which gives a geometric curve representation. In order to link the geometric features of the curve contained in the curvature and torsion to the shape function X of the curve, we first note that the vectors $s \mapsto T(s), N(s), B(s)$ are tightly related through Frenet-Serret ODE

$$\begin{cases} T'(s) = \kappa(s)N(s) \\ N'(s) = -\kappa(s)T(s) + \tau(s)B(s) \\ B'(s) = -\tau(s)N(s) \end{cases} \quad (5)$$

with an initial condition $T(0), N(0), B(0)$. In other words, the moving frame defines a curve $s \mapsto Q(s) = [T(s)|N(s)|B(s)]$ in the group of special orthogonal matrices $SO(3)$ where $SO(p) = \{Y \text{ is a } p \times p \text{ matrix } | Y^\top Y = I_p, \det(Y) = 1\}$. As $SO(3)$ is a Lie group with a manifold structure, the Frenet-Serret ODE can be seen as an ODE defined in the Lie group with

$$Q'(s) = Q(s)A(s) \quad (6)$$

where

$$A(s) = \begin{bmatrix} 0 & -\kappa(s) & 0 \\ \kappa(s) & 0 & -\tau(s) \\ 0 & \tau(s) & 0 \end{bmatrix}, \quad (7)$$

and $A^\top = -A$ so A is skew-symmetric. We shall denote by θ the functional parameters (κ, τ) with the set of admissible parameters by $\mathcal{H} = \{\theta = (\kappa, \tau), \kappa > 0, \kappa, \tau \in C^2\}$, and by A_θ the corresponding skew-symmetric matrix. We call the solutions $s \mapsto Q(s)$ of the Frenet-Serret equations the Frenet paths, and the set of Frenet paths is denoted by

$$\mathcal{F} = \{s \mapsto Q_\theta(s) | Q'(s) = Q(s)A_\theta(s), s \in [0, 1], Q(0) \in SO(3), \theta \in \mathcal{H}\}.$$

Among the set of all Frenet paths, we pay a particular attention to the subset of Frenet paths with initial condition equal to the identity matrix I_3 , $\mathcal{F}_0 = \{Q \in \mathcal{F} | Q(0) = I_3 \in SO(3)\}$. Denote the set of arclength-parametrized regular curves of length 1 by \mathcal{C}_1 . As any regular curve X can be recovered by integrating its tangent $X'(s) = T_\theta(s)$, we have

$$\mathcal{C}_1 = \left\{ s \mapsto X(s) = X_0 + Q_0 \int_0^s T_\theta(u) du \mid Q_\theta \in \mathcal{F}_0, X_0 \in \mathbb{R}^3, Q_0 \in SO(3) \right\} \quad (8)$$

indexed by the parameters (X_0, Q_0, θ) . This parametrization is known to be one-to-one: for any curve X_1 and X_2 having the same curvature and torsion, there exists a vector a and a rotation $R \in SO(3)$ such that $X_1 = a + RX_2$. If the Frenet path for X_2 has an initial condition equal to I_3 , the rotation matrix R is exactly the initial condition of the Frenet path associated with

X_1 . For this reason, the space \mathcal{F}_0 can be naturally considered as the shape space. The functions $s \mapsto \theta(s)$ or $s \mapsto Q_\theta(s)$ represent the geometrical content of any regular curve X .

For regular curves in \mathbb{R}^p for $p > 3$, the same moving frame in $SO(p)$ can be defined, in terms of a skew-symmetric matrix similar to (7), and the so-called generalized curvatures $\kappa_1, \kappa_2, \dots, \kappa_{p-1}$ (Kühnel, 2015).

3.3 Effect of scaling

If we want to consider invariance with respect to rescaling, it suffices to rescale the curves of different length L_i (and arclength s_i) to the same length equal to 1. Rescaling does change the geometry only through a scaling factor, i.e the matrix $s \mapsto A(s)$ in the ODE (6) is also renormalized and the rescaled curves $\frac{1}{L}X(s)$ have new curvilinear arclength $\tilde{s} = s/L$ and the rescaled Frenet paths are $\tilde{Q}(\tilde{s}) = Q(\tilde{s}L)$. The rescaled Frenet-Serret ODE, defined on $[0, 1]$ is $\tilde{Q}'(\tilde{s}) = \tilde{Q}(\tilde{s})\tilde{A}(\tilde{s})$ with $\tilde{A}(\tilde{s}) = LA(\tilde{s}L)$, implying that rescaling a curve by $1/L$, multiplies its curvature and torsion by L .

From now on, we define the equation with the scaled curves to the unit length.

3.4 Problem formulation

Recall that the curves can be expressed as

$$x_i(t) = X_i(s_i(t)), \quad s_i(t) = \int_0^t \|\dot{x}_i(u)\| du, \quad i = 1, \dots, N.$$

As seen in section 3.2, the shape function X_i is associated with an ODE parametrized with respect to functional parameter θ_i :

$$X_i(s) = X_{i0} + Q_{i0} \int_0^s T_{\theta_i}(u) du, \quad Q_i'(s) = Q_i(s)A_{\theta_i}(s).$$

Consequently, we identify the shapes with the Frenet paths $\mathbf{Q} = \{Q_1, \dots, Q_N\}$, or equivalently with the set of curvatures and torsions $\boldsymbol{\theta} = \{\theta_1, \dots, \theta_N\}$. Our aim is then to derive a mean parameter $\bar{\theta}$ (and mean Frenet path \bar{Q}) for \mathcal{S} as a measure of centrality that corresponds to the mean shape defined as

$$\bar{X}(s) = \bar{X}_0 + \bar{Q}_0 \int_0^s T_{\bar{\theta}}(u) du, \quad \bar{Q}'(s) = \bar{Q}(s)A_{\bar{\theta}}(s),$$

which is independent of the variations in translations, rotations and scalings. Our parametrization of curves in (8) shows that the quotient space of arclength parametrized curves (under the group action of Euclidean motions) is exactly the space of Frenet paths. Hence, it is sufficient to work with a population of Frenet paths to define a mean shape.

Contrary to the elastic shape analysis, our focus is not on defining a proper metric on the shape space to define a Fréchet mean. We are interested in developing a statistical characterization of a mean shape that enables us to identify the mean parameter. We do not assume the existence of a generative model for the mean shape or the mean parameter in relation to Q_i or θ_i but directly exploits the characteristic features of the Frenet paths, as the solution of the ODEs, and consider the ODE as a model constraint.

3.5 Mean shape and mean vector field

A fundamental concept for solving an ODE is the flow over time t , denoted by $\phi(t, \cdot)$ (Hairer et al., 2006). It is the mapping that, to each point $Q \in SO(p)$, associates the value of the Frenet paths $Q(t)$ at time t of the solution with initial value $Q(0) = Q$. That is, $\phi(t, Q) = Q(t)$ if $Q(0) = Q$ and t represents the elapsed time. To express the dependence on the initial time, we extend the definition of the flow as $\phi(t, s, Q) = Q(s + t)$ if $Q(s) = Q$ so $\phi(t - s, s, Q) = Q(t)$. The essential property of the flow is the group property, i.e for all $s, u, t \in [0, 1]$ and $Q \in SO(p)$, $\phi(t - s, s, Q) = \phi(t - u, u, \phi(u - s, s, Q))$. This allows us to express any localized solution coherently to the global solution. As the Frenet path is indexed by θ , the corresponding flow is written as ϕ_θ .

We see that the geometrical features θ_i define the vector field $Q \mapsto QA_{\theta_i}(s)$, and that the observable features such as tangent, normal or binormal vectors are in fact the corresponding flows ϕ_{θ_i} . These observations lead us to defining the mean shape as the mean of the vector fields $Q \mapsto QA_{\theta_i}(s)$. We define then the mean vector field as the vector field defined on $SO(p)$ such that the solution paths are close to the individual Frenet paths Q_i , $i = 1, \dots, N$. In other words, the mean vector field corresponds to the flow that provides a *best* approximation to all the individual flows.

A noticeable feature of our formulation is that we do not use the infinitesimal characterization of the differential equation based on the derivative. We use instead the group property of the flow that can be interpreted as a *self-prediction property*: if $s \mapsto Q(s)$ is a solution to equation (6), then for all $t, s \in [0, 1]$ such that $|t - s| \leq 1$, we have

$$Q(t) = \phi_\theta(t - s, s, Q(s)). \quad (9)$$

Otherwise, the curve $s \mapsto Q(s)$ is a solution to $Q' = QA_\theta$ if and only if

$$\int_0^1 \int_0^1 d(Q(t), \phi_\theta(t - s, s, Q(s))) ds dt = 0, \quad (10)$$

where $d(\cdot, \cdot)$ is a distance defined on $SO(p)$. As d is non-negative, it holds also with d^2 in (10). As we want to replace θ_i by a common $\bar{\theta}$, we require that the mean flow $\phi_{\bar{\theta}}$ should minimize the self-prediction errors for all the trajectories simultaneously. The individual error is measured by

$$\mathcal{V}(Q_i, \phi_\theta) = \int_0^1 \int_0^1 d(Q_i(t), \phi_\theta(t - s, s, Q_i(s)))^2 ds dt. \quad (11)$$

Definition 1. Let $Q_i \in SO(p)$, $i = 1, \dots, N$ be the independent and identically distributed random Frenet paths with the same distribution as Q , associated with parameters $\theta_i \in \mathcal{H}$ satisfying $Q'_i = Q_i A_{\theta_i}$. The mean parameter for the Frenet path Q is defined as

$$\bar{\theta} = \arg \min_{\theta \in \mathcal{H}} E\{\mathcal{V}(Q, \phi_\theta)\}.$$

3.6 Estimation of mean parameter

Suppose that we have a sample of Frenet paths $\{Q_1, \dots, Q_N\}$ with the corresponding parameters $\theta_1, \dots, \theta_N$. We develop an empirical criterion to construct an estimator. The essential ingredients of our definition of the mean based on the self-prediction criterion (11) are the distance function d and the representation of the flow ϕ_θ . The choice of these need to be adapted to the underlying sample space.

Due to the orthogonality constraint, the Frenet differential equation is not defined on the Euclidean space but on the special Lie group $SO(p)$. Ensuring the orthogonality constraint requires a special treatment in developing a numerical algorithm to solve an ODE and also in tackling a parameter estimation problem in ODE, as numerical errors can accumulate and induce an uncontrolled bias. The extension of the theory of ODEs from Euclidean space to Lie groups or manifolds is well developed (Hairer et al., 2006). In particular, the rotation group $SO(p)$ is a Lie Group that is also a differentiable manifold, with many remarkable properties that are essential in tackling the numerical problems (Absil et al., 2010).

We first highlight some useful features of the sample space as $SO(p)$, which allows us to define a geodesic distance d and develop a workable representation of the flow ϕ_θ . Based on these, we develop an empirical criterion in the spirit of nonparametric function estimation problem.

3.6.1 Solving ODE on $SO(p)$

Typically, $SO(p)$ is considered as a submanifold of the Euclidean space $\mathbb{R}^{p \times p}$, with the usual inner product $\langle M, N \rangle = \text{Tr}(M^\top N)$ (and the associated Frobenius norm). The Tangent Space at point M to $SO(p)$ is the vector space

$$T_M SO(p) = \{MU | U^\top = -U\},$$

usually identified with the set of skew-symmetric matrices (U). In particular, the Tangent Space at the identity I_p is called the Lie algebra of the Lie group, denoted by $\mathfrak{so}(p)$.

A fundamental tool for the analysis of ODE and flows on Lie groups is the Exponential map, Exp_M , at point M , which relates the tangent space to the manifold. The Exponential map $\text{Exp}_M : T_M SO(p) \rightarrow SO(p)$ is such that $\text{Exp}_M(U) = \gamma(1; M, U)$, where γ is the unique geodesic $s \mapsto \gamma(s, M, U)$ such that $\gamma(0; M, U) = M$ and $\gamma'(0; M, U) = U$. Conversely, if we have a given root M and a target point N , the logarithmic map returns a tangent vector at M , pointing toward N , of length $\text{dist}(M, N)$. Hence, the logarithmic map $\text{Log}_M : SO(p) \rightarrow T_M SO(p)$ at M is $\text{Log}_M(N) = V$ such that $\text{Exp}_M(V) = N$ and $\|\text{Log}_M(N)\| = \text{dist}(M, N)$.

Fortunately, if we consider a matrix Lie group, the exponential and logarithmic maps can be expressed simply with the classical matrix exponential $\exp(A) = \sum_{k \geq 0} \frac{A^k}{k!}$ and matrix logarithm, see Higham (2008). In particular, we have

$$\text{Exp}_M(U) = M \exp(U), \quad \text{Log}_M(N) = \log(M^\top N). \quad (12)$$

As a consequence, the geodesic distance $\text{dist}(M, N) = \|\log(M^\top N)\|_F$ has a closed form expression that is amenable to computation. Numerous efficient algorithms exist for computing the exponential of a matrix; the case of $p = 3$ is remarkable, as in that case the exponential and logarithm have a closed-form expression. We will use in our applications these formulas to derive our fast algorithms.

Now we want to express the flow ϕ_θ of the Frenet ODE on $SO(p)$. An ODE is defined as a function $F : SO(p) \rightarrow T_M SO(p)$, such that $\dot{Y}(t) = F(t, Y(t))$. In the case of the Frenet-Serret equation, the vector field is time-varying but relatively simple. In light of the relation (12), a fruitful approach to solving a differential equation $\dot{Y} = YA(t)$ with $Y(0) = Y_0$ in a Lie group is to look for a solution of the form $Y(t) = Y_0 \exp(\Omega(t))$, which defines the flow. This implies that the function $t \mapsto \Omega(t)$ is defined in $\mathfrak{so}(p)$ and is known to admit the so-called Magnus expansion (chapter IV.7 in Hairer et al. (2006), Iserles et al. (2000))

$$\Omega(t) = \int_0^t A(s) ds - \frac{1}{2} \int_0^t \left[\int_0^\tau A(s) ds, A(\tau) \right] d\tau + \frac{1}{4} \int_0^t \left[\int_0^\tau \left[\int_0^\sigma A(\mu) d\mu, A(\sigma) \right] d\sigma, A(\tau) \right] d\tau + \dots, \quad (13)$$

which can be used to derive efficient integration methods. Additional properties of the matrix exponential are summarized in the supplementary.

As explained in section 3.5, the flow can be generalized to represent initial values at arbitrary time s . For all t, s in $[0, 1]$ and θ in \mathcal{H} , we define the matrix-valued (in $\mathfrak{so}(p)$) function $\Omega(t, s; \theta)$ such that the flow can be written as

$$\phi_\theta : (t, s, Q) \mapsto Q \exp(\Omega(t, s; \theta)) , \quad (14)$$

where $\Omega(t, s)$ is defined by replacing \int_0^t with \int_s^{s+t} in (13) so that $Y(t) = \phi_\theta(t - s, s, Y_0)$ if $Y(s) = Y_0$ and $\Omega(t, s; \theta)$ expresses the dependence on θ .

3.6.2 Estimation criterion

Using the geodesic distance in $SO(p)$, combined with the flow (14), the criterion (11) can be expressed as

$$\mathcal{V}(Q_i, \phi_\theta) = \int_0^1 \int_0^1 \|\log(Q_i(t)^\top Q_i(s) \exp(\Omega(t - s, s; \theta)))\|_F^2 ds dt , \quad i = 1, \dots, N .$$

To allow for variation in the prediction error, we incorporate weights according to the distance to initial values s in evaluating the solution at t and define a weighted criterion:

$$\check{\ell}_{N,h}(\theta) = \frac{1}{N} \sum_{i=1}^N \int_0^1 \int_0^1 K_h(t - s) \|\log(Q_i(t)^\top Q_i(s) \exp(\Omega(t - s, s; \theta)))\|_F^2 ds dt , \quad (15)$$

where $K(\cdot)$ is a kernel function with compact support, e.g. $K(u) = \frac{3}{4}(1 - u)^2 1_{[-1,1]}(u)$ and $K_h(u) = (1/h)K(u/h)$. The kernel $K(\cdot)$ and the bandwidth h define a prediction horizon for the flow. In addition, we introduce a smooth regularization for the functional parameter θ with a penalty term

$$\mathcal{P}_\lambda(\theta) = \lambda \|\theta''\|_2^2 = \lambda \int_0^1 \|\theta''(t)\|^2 dt , \quad (16)$$

and define the empirical criterion as $\check{\mathcal{I}}_{h,\lambda}(\theta) = \check{\ell}_h(\theta) + \mathcal{P}_\lambda(\theta)$.

Definition 2. Let $\{Q_1, \dots, Q_N\}$ be a sample of Frenet paths with parameters of curvature and torsion $\theta_1, \dots, \theta_N$. For a fixed h and λ , the sample mean vector field (or curvature) is defined as the parameter θ that minimizes the global prediction error $\check{\mathcal{I}}_{h,\lambda}(\theta)$.

Our definition can be viewed as a generalization of the mean in the scale-space view in nonparametric curve estimation (Chaudhuri and Marron, 2000; Wei and Panaretos, 2018). The following Proposition shows that the mean vector field exists for any h and λ in great generality, as long as the sample is bounded in L^2 .

Proposition 1. Let Q_1, \dots, Q_N be Frenet paths with parameters θ , such that for all $i = 1, \dots, N$, $\|\theta_i\|_\infty \leq C$. There exists $\check{\theta}_{h,\lambda}$ in \mathcal{H} such that

$$\check{\theta}_{h,\lambda} \in \arg \min_{\theta \in \mathcal{H}} \check{\mathcal{I}}_{h,\lambda}(\theta) .$$

We can also define the mean Frenet Path $\check{Q}_{h,\lambda}(t) = \exp(\Omega(t, 0, \check{\theta}_{h,\lambda}))$ and the corresponding mean shape \check{X} obtained by integrating the gradient. However, it is rather difficult to compute the corresponding mean or to analyze it. Since the expression of Ω is intractable in general,

we further derive a consistent approximations to the flow, by truncating the Magnus expansion, see chapter IV in [Hairer et al. \(2006\)](#). In particular, we use an approximation of order 2, obtained by using a simple quadrature rule with the midpoint and truncating after the first term: $Q_{s+h} = Q_s \exp\left(hA_\theta\left(s + \frac{h}{2}\right)\right)$, i.e. $\phi_\theta(h, s, Q_s) - Q_{s+h} = O(h^2)$. The corresponding approximate flow $\tilde{\phi}_\theta(h, s, Q) = QN_h(s, \theta)$ can be seen as an Euler-Lie method that possesses several interesting features: it respects the $SO(p)$ constraint, has an explicit and pointwise dependence in θ , and the approximation is uniform on $SO(p)$. For this reason, we introduce an approximation, $\mathcal{I}_{h,\lambda}(\theta) = \ell_{N,h}(\theta) + \mathcal{P}_\lambda(\theta)$, to the criterion $\check{\mathcal{I}}_{h,\lambda}$, valid for small h (S2.1 in the supplementary), where

$$\ell_{N,h}(\theta) = \frac{1}{N} \sum_{i=1}^N \int_0^1 \int_0^1 K_h(t-s) \left\| \log \left(Q_i(t)^\top Q_i(s) \exp \left((t-s)A_\theta \left(\frac{s+t}{2} \right) \right) \right) \right\|_F^2 ds dt.$$

The following proposition shows that, at first approximation, our approach is tractable and can be easily understood in terms of the geometry the curves.

Proposition 2. Let Q_1, \dots, Q_N be Frenet paths with parameters $\theta_i, i = 1, \dots, N$ in \mathcal{H} , satisfying $\|\theta_i\|_2^2 \leq \frac{\pi}{2}$. Then, there exists $B > 0$, such that for all $\|\theta\|_2 \leq B$,

$$\check{\mathcal{I}}_{h,\lambda}(\theta) - \mathcal{I}_{h,\lambda}(\theta) = O(h^3).$$

3.7 Extension of mean shape under phase variation

We have characterized the variation of the curves $x_i(t) = X_i(s_i(t))$ in terms of its geometry using curvature and torsion, under M_1 in (4). On the other hand, the shape variation of the curves is often viewed as a curve registration problem (e.g., [Marron et al., 2015](#); [Carroll et al., 2020](#)). For curves x_0 and x_1 , the registration problem is motivated by finding the most appropriate warping $h : [0, T] \rightarrow [0, T]$ such that two curves $x_1(h(t))$ and $x_0(t)$ looks similar. In order to incorporate the registration in our framework with arclength parametrized curves, as M_2 in (4), we consider

$$x_0(t) = X_0(s_0(t)), \quad x_1(h_1(t)) = X_1(s_1(h_1(t))).$$

The corresponding Frenet paths are $Q_0(s_0(t))$ and $Q_1(s_1(h_1(t)))$. Under our framework, it is natural to express the registration problem in terms of the Frenet paths.

Define a space warping diffeomorphism $\gamma : [0, L_0] \rightarrow [0, L_1]$ for any $h \in H_T$ such that $s_1 \circ h = \gamma \circ s_0$. Denote the function space of the space warping diffeomorphisms by Γ_S . Then, the warping problem in x is translated into that of $Q_0(s)$ and $Q_1(\gamma(s))$. That is, for two Frenet paths $Q_0 : [0, L_0] \rightarrow SO(p)$ and $Q_1 : [0, L_1] \rightarrow SO(p)$, the curves are stretched using a diffeomorphism $\gamma : [0, L_0] \rightarrow [0, L_1]$. For length normalised curves, we have $L_0 = L_1 = 1$, see section 3.3.

From section 2.3, the Frenet path $s \mapsto \tilde{Q}_1(s) = Q_1(\gamma(s))$ is also the solution of the following Frenet-Serret ODE:

$$\frac{d}{ds} \tilde{Q}_1(s) = Q_1'(\gamma(s))\gamma'(s) = Q_1(\gamma(s))A_\theta(\gamma(s))\gamma'(s) = \tilde{Q}_1(s)A_{\tilde{\theta}}(s),$$

where

$$\tilde{\theta}(s) = \theta(\gamma(s))\gamma'(s). \tag{17}$$

It also satisfies the self-prediction property: for all $t, s \in [0, 1]$ such that $|t - s| \leq 1$, we have

$$\tilde{Q}_1(t) = \phi_{\tilde{\theta}}(t - s, s, \tilde{Q}_1(s)).$$

The self-prediction error criterion (11) for \tilde{Q}_i can be expressed as

$$\begin{aligned}\mathcal{V}(\tilde{Q}_1, \phi_{\tilde{\theta}_1}) &= \int_0^1 \int_0^1 d(Q_1(\gamma(t)), \phi_{\theta(\gamma)\gamma'}(t, s, Q_1(\gamma(s))))^2 ds dt \\ &= \int_0^1 \int_0^1 d(Q_1(\gamma(t)), \phi_{\theta(\gamma(t) - \gamma(s), \gamma(s), Q_1(\gamma(s))))^2 ds dt.\end{aligned}$$

We define an augmented self-prediction error criterion by

$$\mathcal{V}_2(Q, \phi_{\theta}) = \inf_{\gamma \in \Gamma_S} \mathcal{V}(Q(\gamma), \phi_{\theta(\gamma)\gamma'}).$$

Definition 3. Assume that $Q_i, i = 1, \dots, N$ be the independent and identically distributed random Frenet paths with the same distribution as Q , associated with parameters $\theta_i \in \mathcal{H}$, satisfying $Q'_i = Q_i A_{\theta_i}$. For random space diffeomorphisms $\gamma_i \in \Gamma_S$ identically distributed as γ , let $\tilde{Q}_i = Q_i(\gamma_i)$ be the observed Frenet paths. The mean parameter for \tilde{Q} is defined as

$$\bar{\theta}_2 = \arg \min_{\theta \in \mathcal{H}} E\left\{ \inf_{\gamma \in \Gamma_S} \mathcal{V}(Q(\gamma), \phi_{\theta(\gamma)\gamma'}) \right\} = \arg \min_{\theta \in \mathcal{H}} E\{\mathcal{V}_2(Q, \phi_{\theta})\}.$$

The relation (17) defines a ‘‘spatial’’ or geometric registration based on the family of deformations defined as $\theta \mapsto \gamma \cdot \theta = \gamma' \theta \circ \gamma$, for any increasing diffeomorphism γ . This is a group action, i.e. for all γ_1, γ_2 diffeomorphisms, and any generalised curvature θ , we have

$$(\gamma_2 \circ \gamma_1) \cdot \theta = \gamma_2 \cdot (\gamma_1 \cdot \theta).$$

Note that the stretching action by warping does not permit to transform any geometry into another. Indeed, if θ_0 and θ_1 are two generalised curvatures such that the torsion $\tau_0 > 0$ and $\tau_1 < 0$, then we cannot find γ such that $\gamma' \tau_1(\gamma) = \tau_0$ (Brunel and Park, 2019). Our mean parameter is identified as the solution to a constrained minimization problem.

4 Estimation algorithm

We first derive a main algorithm for estimation under shape variation model and extend it to cover phase variation model. As the Frenet paths are often not directly available, we suggest pre-processing methods to treat the Euclidean curves. Furthermore, as a special case of the Euclidean curves with a manifold structure, we show that our estimation algorithm can be applied to the spherical curves by reparametrization.

4.1 Estimation under shape variation

Based on the statistical criterion developed in section 3.6, the estimation of θ from given Frenet paths \mathbf{Q} is done by solving

$$\hat{\theta}_{h,\lambda}(\cdot) = \arg \min_{\theta} \mathcal{I}_{h,\lambda}(\theta). \quad (18)$$

We need to solve the nonparametric estimation problem (18), but in practice, we solve this by discretization. Suppose that $Q_i, i = 1, \dots, N$ is available at finite grid points $s_{ij}, j = 1, \dots, n_i$. Then we discretize the integral on a grid $0 = t_{i1} < t_{i2} < \dots < t_{iQ_i} = 1$ and minimize

$$\min_{\theta \in \mathcal{H}} \sum_{i=1}^N \frac{1}{n_i Q_i} \sum_{j,q=1}^{n_i, Q_i} K_h(t_{iq} - s_{ij}) \left\| \log \left(Q_i(t_{iq})^\top Q_i(s_{ij}) \exp \left((t_{iq} - s_{ij}) A_{\theta} \left(\frac{t_{iq} + s_{ij}}{2} \right) \right) \right) \right\|_F^2 + \lambda \|\theta''\|_2^2$$

The presence of the exponential makes the optimization difficult, and we use an additional approximation that provides a simple algorithm and simplifies the analysis of our estimator. Let

$$L_{ijq} = \log \left(Q_i(t_{iq})^\top Q_i(s_{ij}) \exp \left((t_{iq} - s_{ij}) A_\theta \left(\frac{t_{iq} + s_{ij}}{2} \right) \right) \right).$$

Define $u_{ijq} = t_{iq} - s_{ij}$, $v_{ijq} = \frac{t_{iq} + s_{ij}}{2}$. The first term in the criterion can be expressed as

$$\sum_{i,j,q=1}^{N,n_i,Q_i} \frac{1}{n_i Q_i} K_h(u_{ijq}) \|L_{ijq}\|_F^2.$$

We define the skew-symmetric matrix $R_{ijq} = -\frac{1}{t_{iq} - s_{ij}} \log(Q_i(t_{iq})^\top Q_i(s_{ij}))$. We derive a first order approximation to $\|L_{ijq}\|_F$ based on the Baker-Campbell-Hausdorff formula (Higham, 2008): for t small enough,

$$\exp(tA) \exp(tB) = \exp \left(tA + tB + \frac{1}{2} t^2 [A, B] + O(t^3) \right).$$

where $[A, B] = AB - BA$. In particular, it can be shown (S2.2 in the supplementary) that

$$\sum_{i,j,q=1}^{N,n_i,Q_i} \frac{1}{n_i Q_i} K_h(u_{ijq}) \|L_{ijq}\|_F^2 = \sum_{i,j,q=1}^{N,n_i,Q_i} \frac{1}{n_i Q_i} K_h(u_{ijq}) u_{ijq}^2 \|A_\theta(v_{ijq}) - R_{ijq}\|_F^2 + O(h^3).$$

This motivates us to introduce a new approximate criterion,

$$\tilde{\mathcal{I}}_{h,\lambda}(\theta; \mathbf{R}) = \sum_{i,j,q=1}^{N,n_i,Q_i} \frac{1}{n_i Q_i} K_h(u_{ijq}) u_{ijq}^2 \|A_\theta(v_{ijq}) - R_{ijq}\|_F^2 + \lambda \int_0^1 \|\theta''(t)\|^2 dt.$$

In the particular case of $p = 3$, if we define

$$R_{ijq} = \begin{bmatrix} 0 & -r_{ijq}^1 & -r_{ijq}^3 \\ r_{ijq}^1 & 0 & -r_{ijq}^2 \\ r_{ijq}^3 & r_{ijq}^2 & 0 \end{bmatrix}$$

the Frobenius norm can be rearranged with weights $\omega_{ijq} = \frac{2}{n_i Q_i} K_h(u_{ijq}) u_{ijq}^2$ using the element-wise expansion, leading to

$$\tilde{\mathcal{I}}_{h,\lambda}(\theta; \mathbf{R}) = \sum_{i,j,q=1}^{N,n_i,Q_i} \omega_{ijq} (\kappa(v_{ijq}) - r_{ijq}^1)^2 + \sum_{i,j,q=1}^{N,n_i,Q_i} \omega_{ijq} (\tau(v_{ijq}) - r_{ijq}^2)^2 + \lambda \int_0^1 \|\theta''(t)\|^2 dt.$$

That is, the optimization problem for $p = 3$

$$\tilde{\theta}_{h,\lambda} = \arg \min_{\theta \in \mathcal{H}} \tilde{\mathcal{I}}_{h,\lambda}(\theta; \mathbf{R})$$

gives rise to the computation of 2 independent smoothing splines (with splines of third order), defined at the knots v_{ijq} , with the pseudo-observations r_{ijq}^1, r_{ijq}^2 . The only difference with respect to the classical smoothing splines is the presence of the weights ω_{ijq} .

Remark 1. Our prediction error depends on $h, \lambda = (\lambda_1, \lambda_2)$. If h is too big, we integrate along the whole interval and the errors accumulate, and it is better to restrict to smaller interval. We consider the prediction of a small percentage (10%, $h \approx 0.1$) of the individuals, when the total length of a curve is 1. In our numerical studies we have performed 10-fold cross validation by minimizing

$$\sum_{k=1}^K \sum_{(i,j) \in T_k} \left\| \log \left(U_{ij}^\top \hat{Q}_i^{-(k)}(s_{ij}; h, \lambda) \right) \right\|_F^2$$

where T_k is the k th index set based on $K = 10$ random partition of the observations $\{U_{ij} = Q_i(s_{ij})\}$, $i = 1, \dots, N, j = 1, \dots, n_i$ and $\hat{Q}_i^{-(k)}(s_{ij}; h, \lambda)$ are the predicted Frenet paths reconstructed with parameters $\hat{\theta}^{-(k)}$, estimated without the k th partition dataset, using hyperparameters h, λ and the initial value of $\hat{Q}(0)$.

4.2 Estimation under phase variation

Under the phase variation model M_2 in (4), the mean parameter needs to be refined to satisfy (17). This is translated into the problem of aligning the raw estimates of the parameters $r_{ijq} = (r_{ijq}^1, r_{ijq}^2)$ to obtain the optimal warping function γ_i . Define $\tilde{R}_{ijq} = \gamma_i(v_{ijq}) \cdot R_{ijq}$ as in (17). Then, the estimates are defined as the minimizer of

$$\tilde{\mathcal{I}}_{h,\lambda}(\theta; \tilde{\mathbf{R}}) = \sum_{i,j,q=1}^{N,n_i,Q_i} \omega_{ijq} (\kappa(v_{ijq}) - \tilde{r}_{ijq}^1)^2 + \sum_{i,j,q=1}^{N,n_i,Q_i} \omega_{ijq} (\tau(v_{ijq}) - \tilde{r}_{ijq}^2)^2 + \lambda \int_0^1 \|\theta''(t)\|^2 dt.$$

For the alignment of the raw estimates, we implement a version of the iterative algorithm similar to those developed in [Kneip and Ramsay \(2008\)](#); [Tucker et al. \(2013\)](#) based on the Kahrnen-Loève expansion : $r_i \circ \gamma_i \approx \nu + \sum_{k=1}^K \xi_{ik} \phi_k$ where ϕ_k are the functional principal components and ξ_{ik} are the corresponding scores. The alignment algorithm is summarized below. The main difference is in step 2 to satisfy (17) with multiplication factor $\dot{\gamma}$ instead of $\sqrt{\dot{\gamma}}$ as in (2).

Alignment algorithm

Given observations $(r_i)_{i=1,\dots,N}$, set the initial values $y_i^0 = r_i, \gamma^0 = id, \nu^0 = \sum_i \omega_i y_i^0$. For $\ell \geq 1$, the optimal warping functions $(\gamma_i)_{i=1,\dots,N}$ are found by iterating the following steps until convergence:

1. Refine y_i : $\tilde{y}_i^{(\ell)} = \nu^{(\ell-1)} + PCAAPPROX(y^{(\ell-1)} - \nu^{(\ell-1)}, K)$
2. Update γ : $\gamma_i^{(\ell)} = \arg \min_\gamma \|\tilde{y}_i^{(\ell)} - (y_i^{(\ell-1)} \circ \gamma) \dot{\gamma}\|_2$ for $i = 1, \dots, N$
3. Update y : $y_i^{(\ell)} = (y_i^{(\ell-1)} \circ \gamma_i^{(\ell)}) \dot{\gamma}_i^{(\ell)}$ for $i = 1, \dots, N$
4. Update ν : $\nu^{(\ell)} = \sum_i \omega_i y_i^{(\ell)}$

4.3 Estimation from noisy Euclidean curves

The Frenet paths Q are usually derived from Euclidean curves by pre-processing. Suppose that the noisy observations $y_j \in \mathbb{R}^3$ satisfy $y_j = X(s_j) + \sigma \epsilon_j, j = 1, \dots, n$, where $X(s)$ has a Frenet path $Q(s)$ solution of the ODE $Q'(s) = A_\theta(s)Q(s)$. We assume that the arclength parametrization can be done relatively easily, by a simple estimate of the first derivative. An added difficulty with this setting is related to defining a preliminary estimate of the Frenet

path. As a preprocessing step, we nonparametrically estimate the higher-order derivatives of X , $X^{(k)}$, $k = 1, 2, 3$ from the noisy observations y_1, \dots, y_n . These derivatives can be very noisy and are used for computing raw estimates $U_j = \hat{Q}(s_j)$, $j = 1, \dots, n$. We consider two methods for deriving these estimates:

$\hat{Q}^{GS}(s)$ obtained by Gram-Schmidt orthonormalization of the frame $[X^{(1)}|X^{(2)}|X^{(3)}]$. The derivatives are estimated by a standard local polynomial of order 4. With the same derivative estimates, we can compute the estimators of the curvature $\hat{\kappa}^{Ext}$ and torsion $\hat{\tau}^{Ext}$ using the extrinsic formulas.

$\hat{Q}^{LP}(s)$ obtained by constrained nonparametric smoothing of X . Instead of the standard local polynomial, we use a local expansion that uses the orthogonal vectors T, N, B :

$$X(s+h) = X(s) + \left(h - \frac{h^3 \kappa^2(s)}{6}\right) T(s) + \left(\frac{h^2 \kappa(s)}{2} + \frac{h^3 \kappa'(s)}{6}\right) N(s) + \frac{h^3 \kappa(s) \tau(s)}{6} B(s) + o(s^3)$$

We find in our numerical studies that \hat{Q}^{LP} outperforms so this is used to construct our estimator.

4.4 Estimation of curves on the sphere

Our formulation does not require specific structure on the Euclidean curves. Nevertheless, it is of interest if our method is applicable to a structured data such as curves on a manifold. Of course, it is possible to estimate the curvature and torsion without additional knowledge on the manifold. However, since curvature and torsion for spherical curves are intrinsically related, direct estimation does not necessarily respect the constraints, but a constrained optimization is not obvious in this setting either. It turns out that, instead of modifying the algorithm, we can reformulate the problem under our Frenet framework for the spherical curves.

We consider a curve α on a sphere of radius R and center $(0, 0, 0)$. By definition we have $\|\alpha(t)\| = R$ for all $t \in [0, T]$. We consider now the curve parametrised by arc length. As for all $s \in [0, L]$, $\|\alpha(s)\| = R$, we have $\langle \alpha(s), \alpha(s) \rangle = R^2$ so $2\langle \alpha(s), \alpha'(s) \rangle = 0$, thus $\alpha(s)$ is orthogonal to $\alpha'(s)$ for all s . We denote $\beta := \alpha'$. We define the spherical unit normal as $\gamma(s) = (1/R)\alpha(s) \wedge \beta(s)$. Since $\|\alpha(s)\|/R = 1 = \|\beta(s)\|$ for all s and the two are orthogonal, $\|\gamma(s)\| = 1$ too.

Definition 4. Define the *geodesic curvature* of a spherical curve $\alpha : [0, T] \rightarrow \mathbb{S}^2$ parametrised by arclength to be

$$k_g(s) = \langle \alpha''(s), \gamma(s) \rangle.$$

The *geodesic curvature* measures the failure of a curve to be a geodesic.

Proposition 3. (Frenet-Serret formula for spherical frames) Let $\alpha : [0, T] \rightarrow \mathbb{S}^2$, unit sphere, be a spherical curve parametrised by arclength. Let $\beta(s) = \alpha'(s)$ and $\gamma(s) = \alpha(s) \wedge \beta(s)$. The vectors (α, β, γ) define the spherical frame and satisfy the following equation with $k_g(s) = \langle \alpha''(s), \gamma(s) \rangle$

$$\begin{cases} \alpha'(s) = \beta(s) \\ \beta'(s) = -\alpha(s) + k_g(s)\gamma(s) \\ \gamma'(s) = -k_g(s)\beta(s) \end{cases}$$

This proposition implies that if one knows the initial position and direction, a given geodesic curvature function $k_g(s)$ determines a unique spherical curve parametrised by arclength. Therefore, we can directly apply our algorithm with the Frenet frame for spherical curves to obtain an estimate of the geodesic curvature \hat{k}_g . Then we reconstruct the curve by solving the spherical Frenet-Serret ODE above. This method ensures that the estimated mean is in \mathbb{S}^2 .

5 Numerical studies

We conduct simulation studies to assess performance of the proposed methods in identifying mean geometry (curvature, torsion) as well as mean shape in finite samples, followed by real data examples.

5.1 Data generating process

We consider the cases of direct observations of Frenet paths and indirect observations from Euclidean curves, possibly contaminated by noise. These are studied under both shape variation (S1) and phase variation (S2) models as defined in (4). Since the mean parameter is not always available, we add a case of Euclidean curves with unknown parameters (S3). We also include an example of spherical curves as a special of Euclidean curves with a manifold structure (S4).

5.1.1 Scenario 1: Shape variation model

The reference shape is defined by $\bar{\kappa}(s) = \exp(\zeta \sin(s))$, $\bar{\tau}(s) = \eta s - 0.5$ with $\zeta = 1$, $\eta = 0.2$ for $s \in [0, 5]$. We simulate a population of random Frenet paths $s \mapsto Q_i(s)$, $i = 1, \dots, N$ generated by random Frenet-Serret equations with random individual shape parameter $\theta_i = (\kappa_i, \tau_i)$ obtained as $\kappa_i = \left| \bar{\kappa} + \sigma_\kappa \zeta_i^1 \right|$, $\tau_i = \bar{\tau} + \sigma_\tau \zeta_i^2$, where ζ_i^1, ζ_i^2 $i = 1, \dots, N$ are centered independent Gaussian processes with (unit) Matérn covariance functions² with $\nu = \frac{5}{2}$ and characteristic length scale $\ell = 1$. We set $\sigma_\kappa = \sigma_\tau = 0.3$. This means that the random functions are twice differentiable, and the functions $\bar{\kappa}, \bar{\tau}$ are respectively the means of the population $(\kappa_i)_{i=1 \dots N}$ and $(\tau_i)_{i=1 \dots N}$. For the Frenet paths, we allow for random initial conditions $Q_i(0) = Q_i^0$ where $Q_i^0 \sim \mathcal{F}(I_3, \alpha_0)$ with $\alpha_0 = 10$, Fisher-Langevin distribution with mean identity and concentration $\alpha_0 = 10$. Denote by X_{θ_i} the corresponding Euclidean curves to Q_i . We consider two types of observations models:

S1.1 Observations as Frenet paths:

$$U_{ij} = Q_i(s_{ij}) M_{ij}, \quad i = 1, \dots, N, j = 1, \dots, n_i,$$

where random rotations $M_{ij} \sim \mathcal{F}(I_3, \alpha)$.

S1.2 Observations as noisy Euclidean curves:

$$y_{ij} = X_{\theta_i}(s_{ij}) + \sigma_e \epsilon_{ij}, \quad i = 1, \dots, N, j = 1, \dots, n_i.$$

5.1.2 Scenario 2: Shape and Phase variation model

The reference shape is defined by $\bar{\kappa}(s) = 10(\sin(3s) + 1)$, $\bar{\tau}(s) = -10 \sin(2\pi s)$ and we set $L = 1$ and $\bar{s}(t) = t$. We simulate a population of Frenet paths $s \mapsto Q_i(s)$, $i = 1, \dots, N$ generated by Frenet-Serret equations with individual shape parameter θ_i obtained as $\kappa_i = \omega_i'(s) \bar{\kappa}(\omega_i(s))$, $\tau_i = \omega_i'(s) \bar{\tau}(\omega_i(s))$, where $\omega_i(s) = \frac{\log(s(\exp(a_i)-1)+1)}{a_i}$ if $a_i \neq 0$ otherwise $\omega_i(s) = s$, and their inverse functions $\omega_i^{(-1)}(s) = \gamma_i(s) = \frac{\exp(a_i s)-1}{\exp(a_i)-1}$ define the space warping functions. We choose a_i equally spaced between -1 and 1 . Similarly to S1, we consider observations as Frenet paths (**S2.1**) and Euclidean curves (**S2.2**) with $s_{ij} = \bar{s}_j$. In addition, we add **S2.3** to emulate time warping in the Euclidean curves.

² $k(s, s') = \frac{1}{\Gamma(\nu)2^{\nu-1}} \left(\frac{\sqrt{2\nu}}{\ell} |s - s'| \right)^\nu K_\nu \left(\frac{\sqrt{2\nu}}{\ell} |s - s'| \right)$

S2.3 Observations as noisy Euclidean Curves with additional time warping: We generate the arclength functions according to

$$s_i(t) = \gamma_i \circ \bar{s} \circ h_i(t), \quad i = 1, \dots, N,$$

where $h_i(t) = b_i \sin(2\pi t) + t$ and b_i are equally spaced between -0.1 and 0.1 so that the functions remain strictly increasing. We have $X_{\theta_i}(s_{ij}) = x_{\theta_i}(t_j)$ with $t_0 < \dots < t_n$ equally spaced between 0 and 1 and the measurement model is defined as

$$y_{ij} = x_{\theta_i}(t_j) + \sigma_e \epsilon_{ij} \quad i = 1, \dots, N, j = 1, \dots, n_i.$$

In S1 and S2, α and σ_e control the noise level in the data respectively.

5.1.3 Scenario 3: Model with unknown parameters

We treat the case where the true mean parameter is implicitly defined. We consider a parametric curve defined by $x_1(t) = \cos(at)$, $x_2(t) = \sin(bt)$, and $x_3(t) = ct$, for $t \in [0, 5]$. We denote by $\varphi = (a, b, c)$ the parameter. The corresponding curvature and torsion are parametric functions of φ . Individual parameters are simulated from $\varphi_i \sim \mathcal{N}(\varphi_{ref}, \sigma_P)$ where $\sigma_P > 0$ is the population variability and $\varphi_{ref} = (1, .9, .8)$. The corresponding curvature and torsion are denoted by θ_{ref} and $\theta_i, i = 1, \dots, N$, respectively. We define the population parameter as $\bar{\theta} \triangleq \frac{1}{N} \sum_{i=1}^N \theta_i$ on $[0, 1]$, and because of the nonlinearity, we have $\bar{\theta} \neq \theta_{ref}$ in general. Nevertheless, when σ_P is relatively small (i.e lower than 0.05 in our case), the geometry of the curves varies but the main features are preserved, meaning the curvatures θ_i varies around θ_{ref} , such that $\theta_{ref} \approx \bar{\theta}$. The measurements are then obtained from $y_{ij} = x_i(t_j) + \sigma_e \epsilon_{ij}, i = 1, \dots, N, j = 1, \dots, n_i$. In the simulation, we vary the model by $\sigma_P^2 = 0.02$ (**S3.1**) or $\sigma_P^2 = 0.05$ (**S3.2**) and the noise level by $\sigma_e^2 = 0$ or $\sigma_e^2 = 0.03$. An example of curves is shown in the supplementary (Figure A).

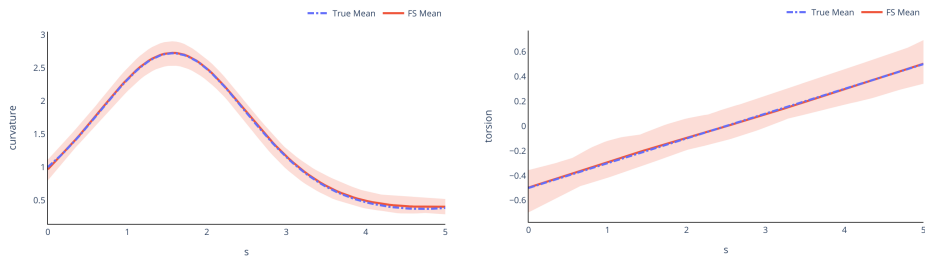
5.1.4 Scenario 4: Model with curves on the sphere

This scenario studies the special case of a population of curves lying on the manifold \mathbb{S}^2 . We consider the generative model for curves on \mathbb{S}^2 described in [Dai and Müller \(2018\)](#). For $i = 1, \dots, N$, the sample curves x_i are generated as $x_i : [0, 1] \rightarrow \mathbb{S}^2, x_i(t) = \exp_{\mu(t)}(\sum_{k=1}^{20} \xi_k \phi_k(t))$ with $\mu(t) = \exp_{[0,0,1]}(\cos(\theta(t))\varphi(t), \sin(\theta(t))\varphi(t), 0)$ the mean function in \mathbb{S}^2 and the arbitrary chosen functions $\theta(t) = 4t + \frac{1}{2}, \varphi(t) = 5(t+1)$. For $k = 1, \dots, 20, \xi_k$ are generated by independent Gaussian distributions with mean zero and variance $0.07^{k/2}$. The functions $\phi_k(t)$ are defined on $[0, 1]$ as $\phi_k(t) = 2^{-1/2} R_t[\Phi_k(t/2), \Phi_k((t+1)/2), 0]^T$, where R_t is the rotation matrix from $[0, 0, 1]$ to $\mu(t)$, and $\{\Phi_k\}_{k=1}^{20}$ is the orthonormal Legendre polynomial basis on $[0, 1]$. The measurements are then obtained from $y_{ij} = x_i(t_j) + \sigma_e \epsilon_{ij}, i = 1, \dots, N, j = 1, \dots, n_i$. For comparison, we identify the true mean parameter $k_g = k_g^\mu$, as defined in section 4.4

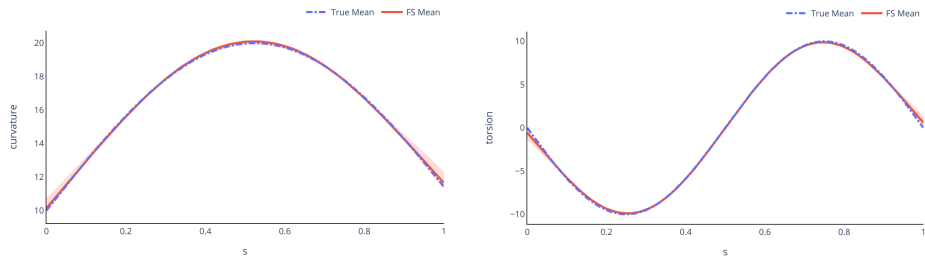
All simulation models are evaluated on a population of $N = 25$ curves with $n = 100$ sample points and are repeated for 100 times. We have run a Bayesian optimization algorithm (e.g., [Martinez-Cantin, 2015](#)) with a standard 10 fold cross validation to search for the best hyperparameters h and λ .

5.2 Simulation results

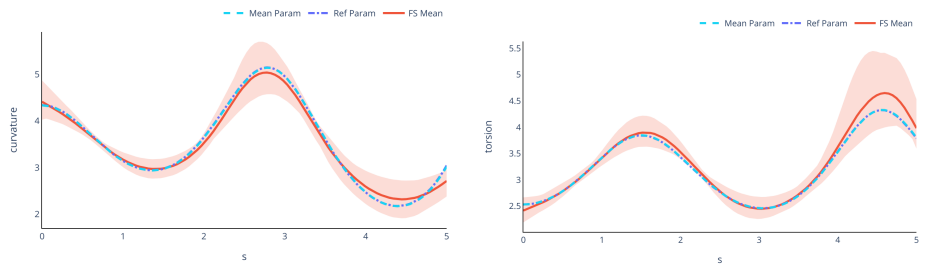
The proposed mean parameter estimate is denoted by $\hat{\theta}^{pop}$. For comparison, we include two alternatives: $\hat{\theta}^{ind}$ defined as the average of the individual estimates by the proposed method,



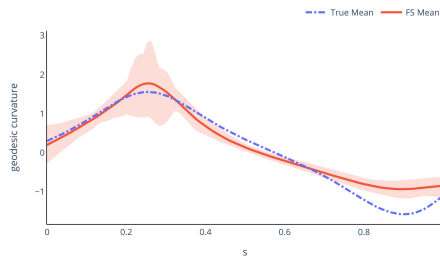
S1.1



S2.1



S3.2



S4

Figure 3: Summary of mean parameter estimates under four scenarios without noise over repetitions. True reference mean parameter is in dash-dotted dark blue and the Frenet-Serret (FS) mean in solid red is the average over 100 repetitions. Shaded regions are the maximum and minimum bounds over repetitions. For S3 the observed mean parameter is shown in dashed light blue line.

and $\hat{\theta}_{Ext}^{ind}$ defined as the median, due to its instability, of the individual estimates computed by extrinsic formulas. The results are summarized in Table 1 with standard errors in parentheses. Figure 3 shows the average values of the estimates, in comparison to the true mean, over 100 repetitions and the shaded areas represent the maximum and minimum bounds.

	error	$\ \hat{\kappa}_{Ext}^{ind} - \bar{\kappa}\ _{L^2}^2$	$\ \hat{\kappa}^{ind} - \bar{\kappa}\ _{L^2}^2$	$\ \hat{\kappa}^{pop} - \bar{\kappa}\ _{L^2}^2$	$\ \hat{\tau}_{Ext}^{ind} - \bar{\tau}\ _{L^2}^2$	$\ \hat{\tau}^{ind} - \bar{\tau}\ _{L^2}^2$	$\ \hat{\tau}^{pop} - \bar{\tau}\ _{L^2}^2$
S1.1	0		0.004 (0.003)	0.004 (0.003)		0.004 (0.003)	0.003 (0.002)
	10		0.009 (0.005)	0.008 (0.004)		0.004 (0.003)	0.004 (0.003)
S1.2	0	11 (2)	0.107 (0.076)	0.102 (0.071)	0.599 (0.118)	0.107 (0.081)	0.089 (0.080)
	0.05	396 (96)	0.594 (0.188)	0.605 (0.228)	18 (7)	2.744 (2.269)	2.139 (2.483)
S2.1	0		0.319 (0.065)	0.021 (0.020)		0.495 (0.092)	0.042 (0.043)
	10		1.158 (0.300)	1.381 (1.456)		1.548 (0.382)	0.573 (0.455)
S2.2	0	39 (2)	0.280 (0.020)	0.028 (0.020)	16 (1)	0.597 (0.005)	0.099 (0.069)
	0.01	61 (12)	1.260 (0.110)	1.182 (0.097)	17 (1)	1.575 (1.293)	1.967 (1.500)
S2.3	0	40 (2)	0.346 (0.024)	0.028 (0.023)	16 (1)	0.791 (0.005)	0.156 (0.063)
	0.01	326 (79)	0.608 (0.300)	0.729 (0.456)	22 (3)	1.691 (1.256)	1.319 (1.355)
S3.1	0	8.001 (0.177)	0.018 (0.005)	0.018 (0.005)	1.633 (0.033)	0.015 (0.006)	0.015 (0.007)
	0.03	$5e^4$ (193)	0.520 (0.316)	0.445 (0.261)	564 (102)	3.636 (2.524)	2.432 (2.211)
S3.2	0	7.785 (0.512)	0.048 (0.027)	0.047 (0.027)	1.686 (0.079)	0.055 (0.048)	0.053 (0.048)
	0.03	$5e^4$ (253)	0.583 (0.416)	0.488 (0.324)	570 (105)	3.793 (2.790)	2.994 (2.790)

Table 1: Estimation errors on mean parameters.

In most cases the results are better with estimation from Frenet paths than from Euclidean curves, the preprocessing required to estimate Frenet paths from curves adds noise which impacts the results. The difference between the individual and global estimates depends very much on the model of the simulation. For **S1**, the variability within the population being more additive, there is no big difference between $\hat{\theta}^{ind}$ and $\hat{\theta}^{pop}$, even if the global estimate remains better. On the contrary, in **S2** with phase warping functions, the results on the case without noise attest to the interest and efficiency of our method with alignment. In noisy cases, it seems that our alignment algorithm suffers, due to the difficulty in alignment with noisy data. This suggests that smoothing methods could be further explored in future development. The results of **S3** show the advantage of global estimation over other types of model. Moreover, we observe that for all the scenarios the torsion is a little more difficult to estimate, as it is linked to the third derivative of the curve which is harder to estimate. Finally, even if we use the same non-parametric estimates of the derivatives, the estimates with the extrinsic formula are very unstable whereas they are much more robust with the proposed method as our approach eliminates oscillations and noise more effectively with a joint estimation of κ and τ , which makes the overall shape more faithful. Additional comparison on the quality of the estimated Frenet paths (Table A in the supplementary) gives a similar conclusion.

The proposed mean shape is denoted by \hat{X}^{FS} . For comparison, we include the elastic mean by SRVF method \hat{X}^{SRVF} described in section 2.4 and the arithmetic mean of Euclidean curves \hat{X}^{Arithm} . The results are visualized in Figure 4. Numerical summaries of L^2 distance as well as Fisher-Rao distance (2) are compared (Table B. in the supplementary). In addition, for curves on the manifold \mathbb{S}^2 (**S4**) we measure how much the mean belongs to \mathbb{S}^2 by $d_{norm}^X = \sum_{j=1}^n |\langle X(s_j), X(s_j) \rangle - 1|$ in Table 2. The L^2 distances are very similar between each method for all scenarios. The Fisher-Rao distance is comparable, and often smaller with the proposed method than with the SRVF method, even though the latter aims to minimize this distance. The arithmetic method also gives better results with the Fisher-Rao distance than the SRVF method in some cases. Overall the distance metrics tend to be similar and do not capture the subtle differences in the geometry very well. Figure 4 shows a large difference in results between **S2.2** and **S2.3**. Both models are the same except that time warping functions are added in **S2.3**. Of

course, as the points are not distributed in the same way along the curve, this affects the result of the arithmetic mean. In contrast to the SRVF method, our method allows the estimation of time warping and space warping functions separately, and therefore gives much better results in this case. Finally, for spherical curves, the shape seems to be well estimated with the SRVF method but the means are no longer on the sphere, contrary to those estimated by our method, which is clearly seen in Table 2. For an adaptation of SRVF method to manifold data, we refer to Su et al. (2014).

σ_e	$\ \hat{k}_{g_{Ext}}^{ind} - \bar{k}_g\ _{L^2}^2$	$\ \hat{k}_g^{ind} - \bar{k}_g\ _{L^2}^2$	$\ \hat{k}_g^{pop} - \bar{k}_g\ _{L^2}^2$	d_{norm}^{FS}	d_{norm}^{SRVF}	d_{norm}^{Arithm}
0	0.137 (0.031)	0.109 (0.043)	0.093 (0.034)	$1e^{-t}$ ($1e^{-t}$)	0.172 (0.019)	0.122 (0.014)
0.02	0.869 (0.777)	0.127 (0.043)	0.109 (0.044)	$3e^{-t}$ ($5e^{-t}$)	0.181(0.014)	0.122 (0.013)

Table 2: Estimation error for spherical curves (S4).

In terms of computational cost, in the setting of these simulations (25 curves, 100 sample points, 80 iterations of Bayesian optimization and 100 repetitions of each simulation) and with fixed hyperparameters, the estimates ($\hat{\theta}$ and \bar{X}) is computed by our algorithm in 1s without phase variation and in about 15s under phase variation (addition of alignment step), when the SRVF method takes about 7s and the Arithmetic method takes 0.1s. These times are given as an indication insofar as the calculation times of these algorithms depend greatly on the parameters of the simulation. The computation times of our algorithm with fixed parameters seem to be of the same order as those of the compared methods, but our method requires several parameters to be optimised in practice, which considerably increases its computational cost. One iteration of Bayesian optimization with 10 fold cross validation takes about 40s, so, as we execute all the repetition in parallel, one simulation scenario with all the optimization process takes about one hour.

5.3 Real data examples

We demonstrate our methodology with two different datasets of human movements shown in Figure 1. For the observed curves x_i , we pre-process the data to create an arclength parametrized data X_i defined on $[0, L_i], i = 1, \dots, n$ and define $Z_i(s) = X_i(sL_i)/L_i, s \in [0, 1]$ as a length-normalized curve. The raw Frenet paths are obtained from a constrained local polynomial smoothing on the normalized domain $[0, 1]$, as \hat{Q}^{LP} in section 4.3.

5.3.1 Mocaplab data: Sign "Fly"

The data set shown in the left of Figure 1 consists of four repetitions of the sign "Fly" in American Sign Language by the same deaf signer, collected by the company MOCAPLAB. In recent years, the company has developed a very precise technique for acquiring finger and hand movements. These data are therefore low-noise. Movements of 3 points on the right hand are recorded and the trajectory of the barycenter of these points constitutes our original data before scaling, visible on the top left of Figure 5. For estimation, the common bandwidth chosen for estimating the raw Frenet paths from constrained local polynomial smoothing is $h_1 = 0.1$ and the hyperparameters are selected from $h \in (0.016, 0.1)$ and $\lambda_1, \lambda_2 \in (1e^{-10}, 1e^{-6})$.

Figure 5 shows three mean shape estimates over the scaled initial data in the left with the parameter estimates in the middle and right. Each Euclidean curve is centred according to its geometric center and the optimal rotation with respect to a reference curve chosen, calculated by Procrustes analysis. On this plot, the SRVF and Arithmetic means appear to have a rather different shape from the replicates and from our mean shape estimate (Frenet-Serret mean). The

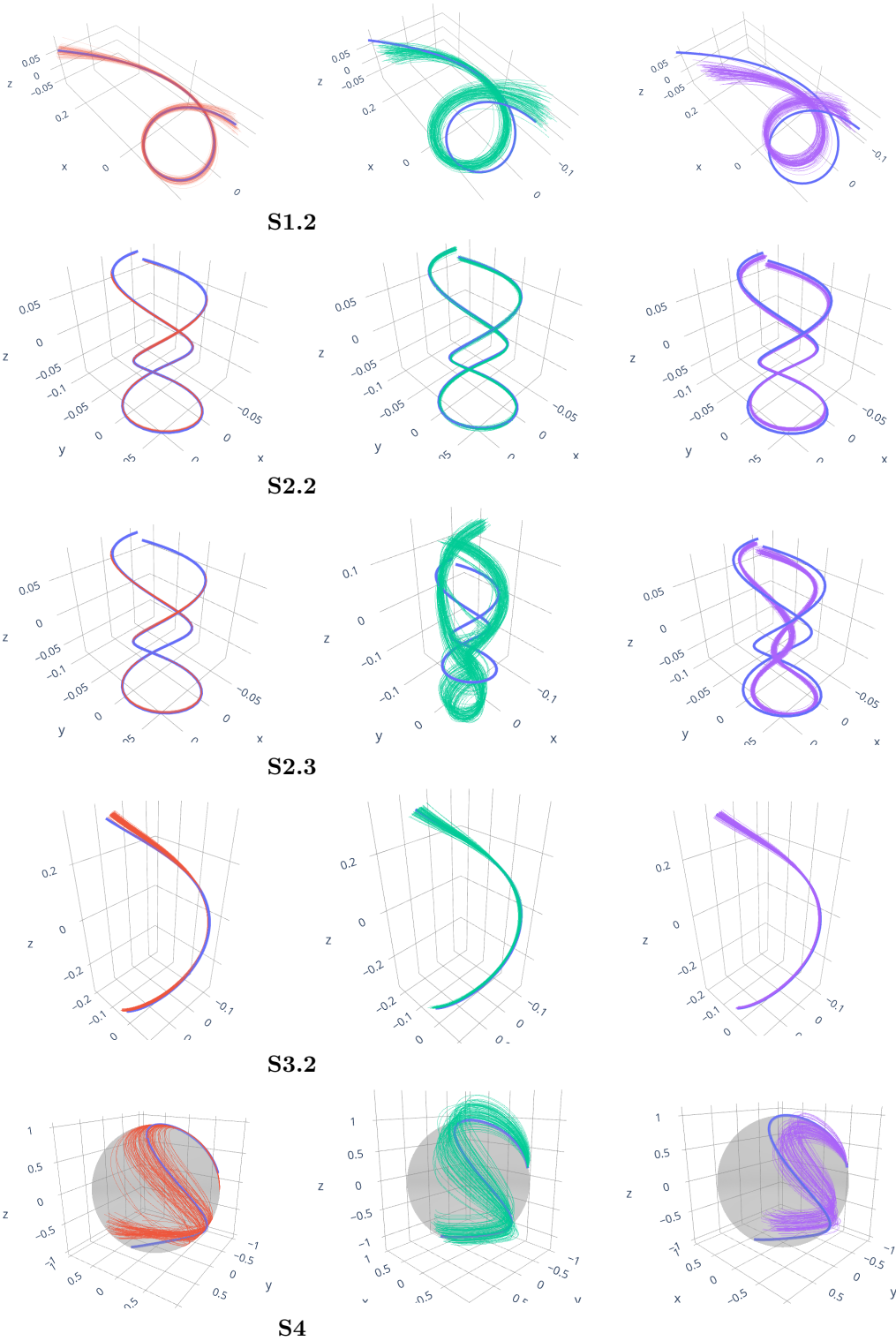


Figure 4: Estimation of mean shape under five scenarios over repetitions, with true mean in blue solid line, Frenet-Serret means in the first column (in red), SRVF means in the middle (in green) and Arithmetic means in the last column (in purple).

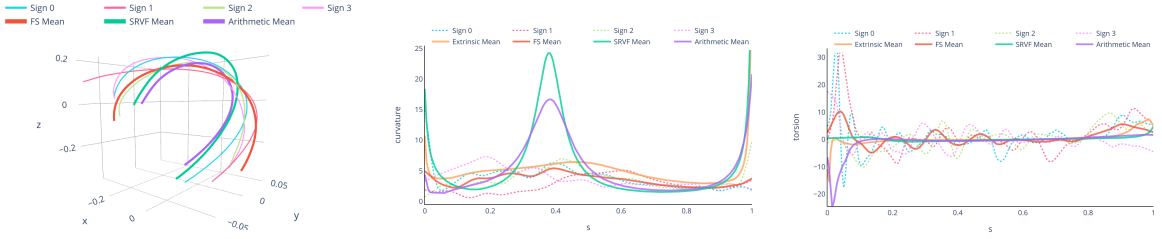


Figure 5: Analysis of trajectories of sign “FLY” shown in Figure 1 left. Three mean shape estimates are shown over scaled trajectories on the left: Frenet-Serret (red), SRVF (green), Arithmetic (purple) means. Frenet-Serret mean curvature (middle) and mean torsion (right) are shown, in comparison with individual estimates. Extrinsic formulas are used to obtain parameters for SRVF and Arithmetic means.

mean Fisher-Rao distance between the estimated mean curve and each initial scaled curve is 0.091 (0.008) for Frenet-Serret mean, 0.285 (0.058) for SRVF mean and 0.271 (0.055) for the Arithmetic mean (resp. for L^2 distance, 0.031 (0.007) for Frenet-Serret, 0.044 (0.009) for SRVF and 0.044 (0.007) for Arithmetic). The corresponding mean curvature and mean torsion ($\hat{\theta}^{pop}$) are plotted, over the individual estimates $\hat{\theta}_i$ and the mean of the individual extrinsic estimates ($\hat{\theta}_{Ext}^{ind}$). For comparison, we also add the curvatures and torsions of the SRVF and the Arithmetic means computed by extrinsic formulas. The curvature profiles confirm the observation already made on the Euclidean curves. Indeed, the curvatures of the SRVF and the arithmetic mean show a broad peak that is not present in the individual curvatures and the torsion curves are quite flat compared to the individual ones, while the curvature and torsion of the Frenet-Serret mean show variations much more similar to the individual curves. This is similar to the example case with torsion variability in Section 2.5.

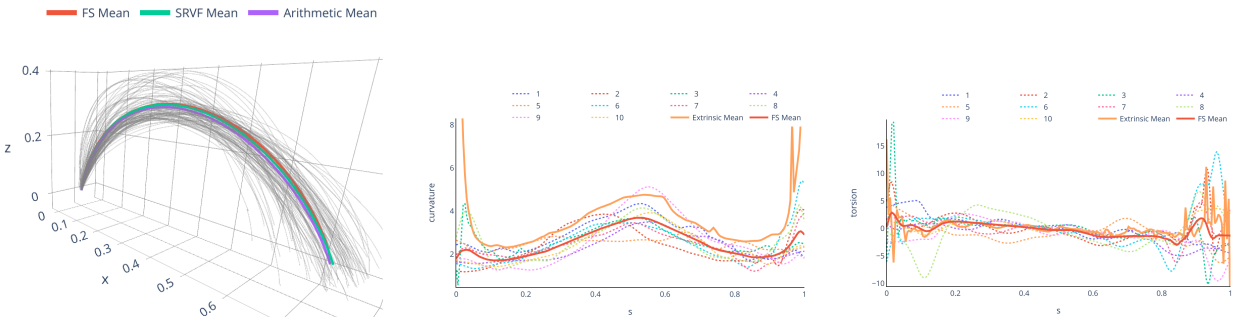


Figure 6: Analysis of trajectories of hand movement shown in Figure 1 right. Results are for 10 participants with 10 repetitions under Condition 8. Three mean shape estimates, Frenet-Serret (red), SRVF (green) and Arithmetic (purple) means are shown over scaled curves (left). Frenet-Serret mean curvature (middle) and mean torsion (right) per participant are shown, in comparison to individual estimates (dotted) and the extrinsic mean estimates (orange).

5.3.2 Raket et al. data

The data set shown in the right of Figure 1 are from a biomedical experiment on hand movement in Raket et al. (2016). An experiment is designed to require each participant to move a hand-held object to a target location while avoiding an obstacle. The trajectories of the (three-dimensional) arm movement of each participant are recorded under various experimental conditions, with an aim to characterize the commonality and variations.

For each condition, we estimate the mean over the 10 different participants and their 10 repetitions. A common bandwidth ($h_1 = 0.2$) is chosen to obtain the raw Frenet paths from constrained local polynomial smoothing. The hyperparameters are selected from $h \in (0.01, 0.1)$ and $\lambda_1, \lambda_2 \in (1e^{-9}, 1e^{-7})$.

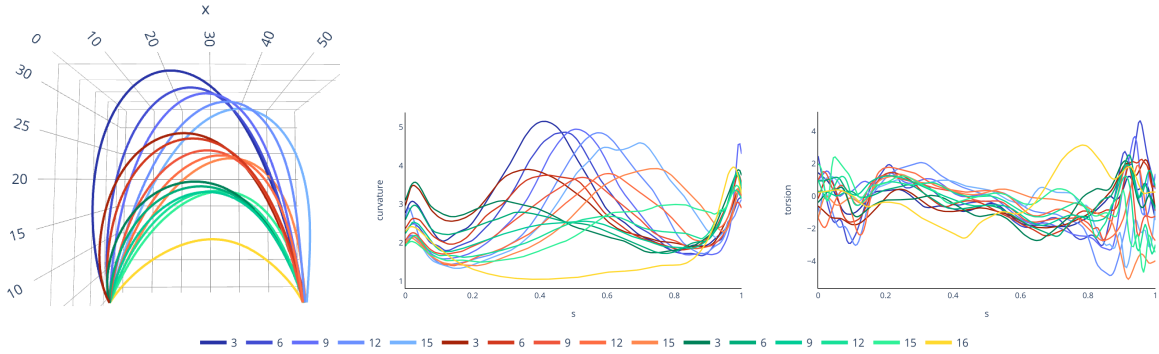


Figure 7: Comparison of mean estimates per condition for hand movement trajectories: mean shape (left), mean curvature (middle) and mean torsion (right). Conditions with tall obstacle are plotted in blue, with medium obstacle in red, small one in green and control condition (without obstacle) in yellow.

Figure 6 presents results from one representative case (Medium obstacle at distance 30.0 cm), of 10 repetitions of 10 participants (one colour per participant). The same data, scaled, are visible in grey on the left of Figure 6, on which the three estimated mean shapes (SRVF, Arithmetic, Frenet-Serret) have been displayed. On the middle and right are shown the proposed mean curvature and mean torsion estimates (red solid), over the mean per participant (dotted). We add the mean of extrinsic estimates (orange solid) for comparison. It can be seen that there is not much variation in amplitude and phase between the different mean parameters per participant. This could explain why the three estimated means are very similar in shape.

In Figure 7 we compare the proposed mean estimates (Euclidean curve, curvature, torsion) for each condition, over all subjects and their repetitions. It appears that the curvatures reflect very well the different distances and heights of the obstacles in each condition, while the torsions are rather similar across all conditions and do not allow to differentiate the three heights for example. We observe a huge difference on curvature and torsion plot, between the control condition done without any obstacle in yellow and the others. This example shows the interest of a method for estimating the mean geometry as well as the mean shape. These additional estimates and information could be used in a complex model of variance analysis (e.g., Backenroth et al., 2018) and this would be an interesting direction to explore for future work.

References

- Absil, P.-A., R. Mahony, and R. Sepulchre (2010). *Optimization On Manifolds: Methods And Applications*. Princeton University Press.
- Backenroth, D., J. Goldsmith, M. D. Harran, J. C. Cortes, J. W. Krakauer, and T. Kitago (2018, jul). Modeling Motor Learning Using Heteroscedastic Functional Principal Components Analysis. *Journal of the American Statistical Association* 113(523), 1003–1015.
- Brunel, N. and J. Park (2019). The frenet-serret framework for aligning geometric curves. In F. Nielsen and F. Barbaresco (Eds.), *Geometric Science of Information*, pp. 608–617. Springer.
- Carmo, M. P. d. (1976). *Differential geometry of curves and surfaces*. Prentice-Hall.
- Carroll, C., H. G. Müller, and A. Kneip (2020). Cross-component registration for multivariate functional data, with application to growth curves. *Biometrics*.
- Chaudhuri, P. and J. S. Marron (2000). Scale space view of curve estimation. *The Annals of Statistics* 28, 408–428.
- Chen, D. and H. Müller (2012). Nonlinear manifold representations for functional data. *The Annals of Statistics* 40, 1–29.
- Chiou, J.-M., Y.-T. Chen, and Y.-F. Yang (2014). Multivariate functional principal component analysis: A normalization approach. *Statistica Sinica* 24, 1571–1596.
- Dai, W. and M. G. Genton (2018). Multivariate functional data visualization and outlier detection. *Journal of Computational and Graphical Statistics* 27(4), 923–934.
- Dai, X. and H.-G. Müller (2018). Principal Component Analysis for Functional Data on Riemannian Manifolds and Spheres. *The Annals of Statistics* 46, 3334–3361.
- Ding, A. and H. Wu (2014). Estimation of ordinary differential equation parameters using constrained local polynomial regression. *Statistica Sinica* 24, 1613–1631.
- Dryden, I. and K. Mardia (1998). *Statistical shape analysis*. Wiley Series in Probability and Statistics. Wiley.
- Dubey, P. and H. G. Müller (2019). Fréchet analysis of variance for random objects. *Biometrika* 106(4), 803–821.
- Ferraty, F. and P. Vieu (2006). *Nonparametric functional data analysis*. Springer Series in Statistics. New York: Springer. Theory and practice.
- Flash, T. and N. Hogan (1985). The coordination of arm movements: an experimentally confirmed mathematical model. *The Journal of Neuroscience* 5(7), 1688–1703.
- Gibet, S., F. Lefebvre-Albaret, L. Hamon, R. Brun, and A. Turki (2016). Interactive Editing in French Sign Language Dedicated to Virtual Signers: Requirements and Challenges. *Universal Access in the Information Society* 15(4), 525–539.
- Goldsmith, J. and T. Kitago (2016). Assessing systematic effects of stroke on motor control by using hierarchical function-on-scalar regression. *Journal of the Royal Statistical Society. Series C: Applied Statistics* 65(2), 215–236.

- Hairer, E., C. Lubich, and G. Wanner (2006). *Geometric Numerical Integration: Structure-Preserving Algorithms for Ordinary Differential Equations*. Springer Series in Computational Mathematics. Springer.
- Happ, C. and S. Greven (2018). Multivariate Functional Principal Component Analysis for Data Observed on Different (Dimensional) Domains. *Journal of the American Statistical Association* 113(522), 649–659.
- Higham, N. (2008). *Functions of matrices: theory and computation*. SIAM.
- Iserles, A., H. Munthe-Kaas, S. Norsett, and A. Zanna (2000). Lie-group methods. *Acta Numerica* 9, 215–365.
- Kim, K. R., I. L. Dryden, H. Le, and K. E. Severn (2021). Smoothing splines on Riemannian manifolds, with applications to 3D shape space. *Journal of the Royal Statistical Society. Series B: Statistical Methodology* 83(1), 108–132.
- Kim, K.-R., P. Kim, J.-Y. Koo, and M. Pierrynowski (2013). Frenet-serret and the estimation of curvature and torsion. *IEEE Journal of Selected Topics in Signal Processing* 7(4), 646–654.
- Kneip, A. and T. Gasser (1992). Statistical tools to analyze data representing a sample of curves. *The Annals of Statistics* 20, 1266–1305.
- Kneip, A. and J. O. Ramsay (2008). Combining registration and fitting for functional models. *Journal of the American Statistical Association* 103(483), 1155–1165.
- Kühnel, W. (2015). *Differential geometry*, Volume 77. American Mathematical Soc.
- Kurtek, S., A. Srivastava, E. Klassen, and Z. Ding (2012). Statistical modeling of curves using shapes and related features. *Journal of the American Statistical Association* 107(499), 1152–1165.
- Lewiner, T., J. Gomes, H. Lopes, and M. Craizer (2005). Curvature and torsion estimators based on parametric curve fitting. *Computers & Graphics* 29(5), 641–655.
- Lin, Z. and F. Yao (2019). Intrinsic Riemannian functional data analysis. *The Annals of Statistics* 47(6), 3533–3577.
- Marron, J. S., J. O. Ramsay, L. M. Sangalli, and A. Srivastava (2015). Functional data analysis of amplitude and phase variation. *Statistical Science* 30(4), 468–484.
- Martinez-Cantin, R. (2015). BayesOpt: A Bayesian optimization library for nonlinear optimization, experimental design and bandits. *Journal of Machine Learning Research* 15, 3735–3739.
- Müller, H.-G. and F. Yao (2010). Empirical dynamics for longitudinal data. *Annals of Statistics* 38(6), 3458–3486.
- Petersen, A. and H. G. Müller (2019). Fréchet regression for random objects with Euclidean predictors. *The Annals of Statistics* 47(2), 691–719.
- Raket, L. L., B. Grimme, G. Schöner, C. Igel, and B. Markussen (2016). Separating timing, movement conditions and individual differences in the analysis of human movement. *POLS Computational Biology* 12(9), 1–27.
- Ramsay, J. and G. Hooker (2017). *Dynamic Data Analysis: Modeling Data with Differential Equations*. Springer Series in Statistics.

- Ramsay, J., G. Hooker, J. Cao, and D. Campbell (2007). Parameter Estimation for Differential Equations: A Generalized Smoothing Approach. *Journal of the Royal Statistical Society (B)* 69, 741–796.
- Ramsay, J. and B. Silverman (2005). *Functional data analysis* (Second ed.). Springer Series in Statistics. Springer.
- Sangalli, L., P. Secchi, S. Vantini, and A. Veneziani (2009). Efficient estimation of three-dimensional curves and their derivatives by free knot regression splines, applied to the analysis of inner carotid artery centrelines. *Journal of the Royal Statistical Society Ser. C, Applied Statistics* 58(3), 285–306.
- Srivastava, A. and E. Klassen (2016). *Functional and shape data analysis*. Springer Series in Statistics. Springer.
- Srivastava, A., E. Klassen, S. Joshi, and I. Jermyn (2011). Shape analysis of elastic curves in euclidean spaces. *IEEE Transactions on Pattern Analysis and Machine Intelligence* 33(7), 1415–1428.
- Su, J., S. Kurtek, E. Klassen, and A. Srivastava (2014). Statistical analysis of trajectories on riemannian manifolds: Bird migration, hurricane tracking and video surveillance. *Annals of Applied Statistics* 8(1), 530–552.
- Tucker, J., W. Wu, and A. Srivastava (2013). Generative models for functional data using phase and amplitude separation. *Computational Statistics and Data Analysis* 61, 50–66.
- Tucker, J. D. (2021). `fdasrsf`: Python package for elastic functional data analysis.
- Wang, J., J. Chiou, and H. Müller (2016). Functional data analysis. *Annual Review of Statistics and Its Application* 3, 257–295.
- Wei, S. and V. M. Panaretos (2018). Empirical evolution equations. *Electronic Journal of Statistics* 12(1), 249–276.
- Younes, L. (2010). *Shapes and diffeomorphisms*. Applied Mathematical Sciences. Springer.